Eur. Phys. J. Plus (2025) 140:384
https://doi.org/10.1140/epjp/s13360-025-06284-2

THE EUROPEAN
PHYSICAL JOURNAL PLUS

Regular Article

Silver/dyes decoupling and colour restoration of autochromes using multispectral imaging

Irina Ciortan[a], **Yoko Arteaga**[b], **Giorgio Trumpy**[c]

Colourlab, Department of Computer Science, NTNU-Norwegian University of Science and Technology, Teknologivegen 22, 2815 Gjøvik, Innlandet, Norway

Received: 18 November 2024 / Accepted: 29 March 2025
© The Author(s) 2025

Abstract Autochrome glass plates, patented in 1903, are one of the earliest colour photography processes. By overlaying a silver emulsion and a screen of randomly placed minuscule starch granules, coloured with orange-red, green and violet-blue dyes, colour images were obtained. Historically, autochromes were viewed by means of light projection, which led to the alteration of the trichromatic screen due to the low lightfastness of the colour dyes. In this article, we propose two methods for the colour restoration of commercially available autochrome plates. Consisting in virtually separating the colour mosaic layer from the silver emulsion, the first approach uses band subtraction to isolate the individual colour dyes, and the second approach is based on linear spectral unmixing. The restoration approaches showcase the colour revival of autochrome plates that enhance the colours and uncover faded details in these historic photographs. The decoupled silver and dye images were also reproduced as translucent prints and integrated into an interactive museum display, allowing visitors to engage with the restored autochrome photographs in a tangible way.

1 Introduction

In 1903, the Lumiere Autochrome revolutionized photography by introducing the first commercially successful colour photography process. Autochrome plates, now housed in a range of museum collections internationally, were the preferred medium of some of the most well-known photographers of the time, such as Alfred Stieglitz [1], Heinrich Kuehn [2], Arthur Huebl [2], Hugh C. Knowles [3], and Karel Smirous [4].

The process comprises a glass plate, on top of which sits a colour filter mosaic made of microscopic starch granules dyed orange-red, green, and violet-blue with carbon filling in-between, and a panchromatic silver gelatine emulsion. Building on James Maxwell's theory of trichromatic human colour vision, late 19th century engineers were experimenting with the implementation of various colour filters (also known as colour screens) with different geometric arrangements [4]. These colour filters can be considered the precursors of the trichromatic filter array currently used in digital colour cameras. What made the colour screens in autochromes stand out from its contemporary rivals (such as the colour screens designed by John Joly and Louis Dufay [4]) was the random distribution of the colour cells, which gave them a more realistic appearance than the otherwise regular patterns. Moreover, the minuscule size of the granules conveyed a distinct pointilistic aesthetic that although appears grainy from up-close, facilitates a natural looking scene when viewed from far-away due to optical mixing [2].

However, the extreme light-sensitivity of these photographs [5] causes the fading of their colours. Autochromes are also susceptible to damage from humidity and moisture, causing dye bleeding and silver layer alteration. Being a glass-based process, they are prone to cracks and fracturing. Because of this sensitivity and fragility, only facsimiles are displayed nowadays in public institutions. Therefore, it is necessary to develop non-invasive tools and methods that enable new ways of public access and digital perusal. In this sense, the main contribution of this work is to present a novel approach for digitizing autochromes that simultaneously enables the restoration of the dyes to their original colours, in a physically based manner.

In this paper, we use a high-resolution, multispectral imaging system to acquire images of four autochromes, purchased from private collections for the purpose of the current research. To begin with, we capture high-resolution multispectral images that can spatially resolve the small colour grains and spectrally characterize the dyes. In our first approach, we exploit the transparency of the dyes in the near-infrared range to capture the silver signal and isolate the signal of the coloured starch elements. Then, in our second approach, we apply linear spectral unmixing in the absorbance domain, where we consider as endmembers the three colour dyes. As

[a] e-mail: irina-mihaela.ciortan@ntnu.no (corresponding author)
[b] e-mail: yoko.arteaga@ntnu.no
[c] e-mail: giorgio.trumpy@ntnu.no

a result of both our decoupling methods, we obtain a map of the colour mosaic elements devoid of the silver emulsion's influence. Afterwards, we replace the spectra of the faded dyes in each autochrome with that of reference, unfaded dyes and recombine them with the silver emulsion.

2 Related works

Over time, the dyes in the colour layer of the autochromes fade, while the silver photographic emulsion remains relatively stable [6] and so does the carbon filling. Particularly, prolonged exposure to intense illumination in non-anoxic conditions generally results in a loss of colour saturation [7, 8], although the image contrast, maintained by the silver particles and the carbon black spaces, remains intact. Casella et al. [7] created fresh samples with all the autochrome dyes, induced light ageing in anoxic and non-anoxic conditions, and spectrally measured the samples before and after ageing. During light ageing, the most fugitive colour grains are the violet-blue ones [9, 10], which are a mix of two dyes (crystal violet and methylene blue), followed by the orange-red grains (a mix of tartrazine, eosin and rose Bengal). Conversely, during dark ageing, when there is no exposure to light, the green-coloured grains (a combination of tartrazine and Patent blue) are the least resistant [2]. After both light and dark ageing, the colours of the autochromes change not only in saturation, but also in hue, and there is usually a shift to a general warmer hue [2, 9, 11].

A pioneering approach for the colour reconstruction of autochromes was proposed by Günzl [11]. He designed an imaging setup with a resolution of 2μm/pixel, which is the minimum necessary to resolve the individual colour grains, as recommended by Lavédrine [12]. A CCD camera was used in combination with three narrow-band interference filters (red, green, and blue) that could separate three groups of colours in the autochrome. However, due to the fading, the three intensity images captured with each filter do not necessarily correspond to the red, green, and blue dyes of the autochrome. For this reason, the space given by the three channels is remapped into a set of 2D coordinates that reduces the cross-talk between the captured channels and facilitates the clustering of the three dyes. Another cluster is considered, represented by the carbon black spaces in-between the colour grains, and it is segmented based on the carbon's low brightness, which is approximately a third of the total average brightness of the autochrome. This thresholding approach is employed here because the black spaces are too small to be resolved by the already high resolution of the imaging system. After the separation of the three dyes, the author assigns new colour values, by applying a colour transformation matrix created from a set of CIE L^*, a^*, b^* measurements collected by Lavédrine [12] from ten autochrome plates. Such a colour correction approach that employs colour correction matrices and a colour adaptation transform was used as well by Pfluger et al. [13] for the visualization of reconstructed lenticular films. Nonetheless, Günzl concludes that the reconstruction is not of a completely objective nature as it includes empirical choices tailored to each autochrome plate and is carried out on a case-by-case basis.

Later, in 1997, Arai et al. [10] compared spectrally and colorimetrically two autochrome plates: one in good condition—not faded, and another one which presents colour deterioration. They take measurements at a microscopical level of the granules in each colour group for the two autochrome plates. In their comparison, they confirm a higher colour difference for the blue granules, as previously found by Lavedrine [12]. In addition, they plot the gamuts of the two autochromes in the CIE xy chromaticity diagram and discover that their primaries are close to the NTSC colour space defined for television. This is especially obvious for the coordinates of the unfaded autochrome, which are closer to the NTSC primaries than the faded autochrome.

Barker et al. [14] and Hubicka et al. [15] have previously attempted restoration of early colour photograph plates by exploiting the geometrical arrangement of additive colour screens, and have developed an open-source tool for this purpose, called ColorScreen. Their restoration method is optimal for photographs with regular colour patterns such as Dufay, Finlay and Paget, which can be synthetically rendered with a simulation model. More precisely, after a preliminary geometrical registration of the regular colour screen with the silver image layer, they are able to characterize the geometric parameters of the colour granules and their location and re-render them with reference CIE xy chromaticities of unaged colour screens, taken from previous research. However, their method is less suitable for photographic plates with random colour arrangement, as is the case of autochromes. Nonetheless, prior to the restoration, Barker et al. used infrared imaging to isolate the silver emulsion layer, because the organic dyes in the early colour photographs, regardless of the nature of the colour pattern, are transparent under infrared radiation.

3 Materials and methods

We propose two methods for the colour restoration of autochromes. Both methods share a common general pipeline sketched in Fig. 1 that starts with the separation of the colour mosaic from the silver emulsion, and then replaces the silver-decoupled dyes with unfaded dyes towards colour restoration. What is distinct in the two methods is the rationale behind the silver/dye separation. The first one uses the disappearance of the dyes in the infrared to decouple the silver emulsion from the colour screen, and so is somewhat similar to the approach of Hubicka et al. [15]. Nonetheless, differently from Hubicka et al. [15], the performance of our method is not influenced by the nature and the regularity of the geometric pattern in the colour screen, and can be applied to autochromes as well as any other type of photography based on additive synthesis. Our second method brings to fruition the spectral resolution of our system by treating the silver/dye decoupling problem as a spectral unmixing task. After the unmixing, we substitute the spectra

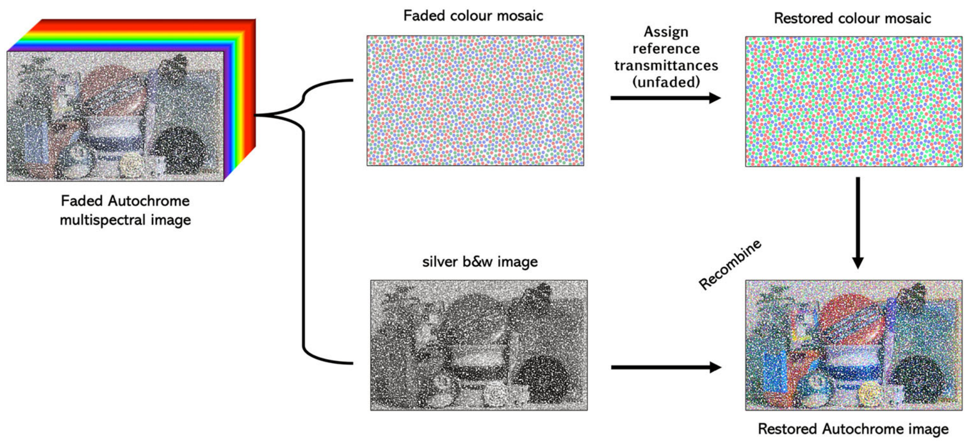

Fig. 1 Our restoration pipeline is defined by the processing of the colour mosaic after its disentaglement from the silver emulsion layer

Fig. 2 Test autochromes acquired for this research (Images not to scale)

(a) Couple by the lake. Autochrome used by permission of the collector, Arthur Clay.

(b) Gruyere, 1914

(c) Harrogate shop window

(d) Poppy field

of the current-state dyes in the colour filter with the spectral signals of reference, unfaded dyes. Consequently, we remix the new, restored colour mosaic with the current-state silver emulsion. To the best of our knowledge, we are the first to solve the restoration of autochromes with a spectral unmixing technique.

3.1 Selection of test autochromes

Autochromes are considered *extraordinarily* light-sensitive materials, and the *Guidelines for Exhibition Light Levels for Photographic Materials* suggest that only facsimiles should be displayed [5]. Autochromes in public museum collections have very restricted access and analyses are limited. Even though our proposed method is a non-contact analysis, the exposure of autochromes to light may accelerate their ageing and colour fading. For this reason, we have acquired a selection of autochromes from private vendors such as photographic antique boutiques and collectors.

Here, we use four autochromes with various sizes, provenance and varying image content (Fig. 2). The autochromes present varying degrees of fading as well as some degradation phenomena common in autochromes, such as greening.

3.2 Spectrophotometric characterization of the test autochromes

Our test autochromes have various origins, different ageing states, and most probably, different manufacturers. This variability makes it valuable to perform spectrophotometric point measurements of their colour primaries at full spectral resolution (ca. 2 nm). For this purpose, the selected autochrome plates were analysed using a custom-built point-based micro-spectrophotometer. The

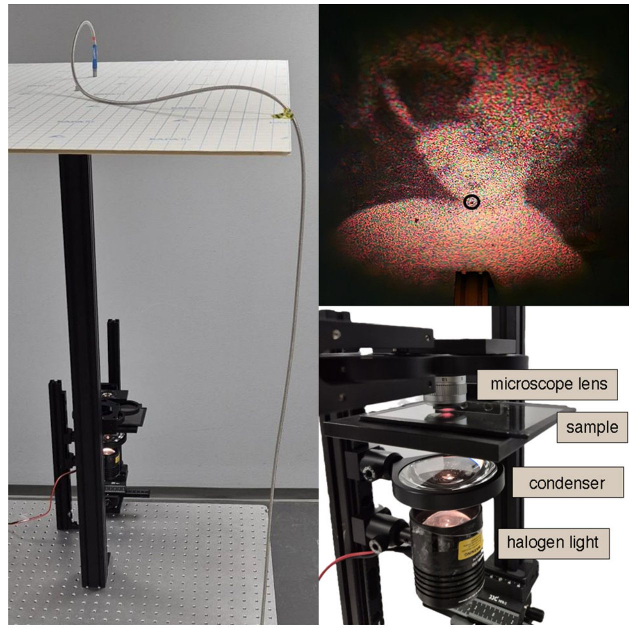

Fig. 3 Overall point measurement spectrophotometric system (left), the image-forming optical components (bottom-right), and the projected image on the foamboard (top-right) of a detail from the "Harrogate shop window" autochrome. The emerging fibre optic is highlighted by a black circle in the projected image

measurement system (shown in Fig. 3) consisted of a Quartz Tungsten–Halogen lamp, two condensing lenses, a 40× microscope objective (Leica HC PL Fluotar), a fibre optic spectrophotometer (Ocean Optics USB2000+XR1-ES) with a measurement aperture of 400 µm, an *XYZ* linear stage, and a white foamboard. The microscope objective projects a magnified image of the illuminated autochrome plate onto the foamboard, through which the fibre optic is inserted. By adjusting the position of the plate using the linear stage, individual colour granules can be measured for spectral radiance and transmittance, with the corresponding bare light radiance serving as a reference.

3.3 High-resolution multispectral image capture

Multispectral images of the test autochromes were captured. The individual colour cells in autochromes, made of dyed potato starch granules, are minuscule with a diameter of approximately 10 µm. Hence, to resolve the single granules, we capture the autochromes with a high-magnification imaging system that allows a spatial resolution on the object plane of 1.84 µm. In addition, for the two silver/dye decoupling methods we propose in the present article, the system has to capture three monochromatic images corresponding to the R, G, B colours plus an image in the near-infrared spectral region. Additionally, a set of images that densely span the full visible range allow us to accurately render true colours. To this purpose, we opted for an active multispectral imaging system, a modified version of the one presented in [16], which consists of a monochrome 16-bit CCD camera and a 5x magnification lens, coupled to an integrating sphere with ten LEDs (see Fig. 4a). The setup captures the transmittance information of the autochrome plates under visible and near-infrared radiation at 10 spectral bands, which corresponds to the following emission peaks of the LEDs (Fig. 5b: 415 nm, 446 nm, 466 nm, 492 nm, 520 nm, 543 nm, 599 nm, 626 nm, 658 nm, and 940 nm. The outgoing light of the integrating sphere is collimated using a condenser lens and then diffused with a translucent slab, creating a diffused bright-field setup. The autochrome is placed on a holder which has a black cover (Fig. 4b), so only the area to be captured is exposed, to limit the light exposure of the autochrome and unwanted stray light. This holder is attached to an *XYZ*-stage, which allows for small displacements to capture tiles of the autochrome which can then be stitched. The exposure time of the captures is set per band, using an optimization method which ensures that the histogram of a white target is maximizing the 16-bit dynamic range without reaching saturated levels. Given the well-known overall low transmittance factor [4] of autochrome glass plates, we use as "white" reference a neutral density (ND) filter of 0.4 optical density, instead of the empty gate. Each of the ten images undergoes flat-fielding and dark current correction, calculating $I_{\text{corrected}} = (I_{\text{captured}} - I_{\text{black}})/(I_{\text{white}} - I_{\text{black}})$, where I_{white} are the images captured through the ND filter.

Given that the subject of the study is an extremely light-sensitive photograph, we aimed to assess the potential impact of light exposure from our method. The light dosage for the capture has been calculated for each spectral band independently, since the exposure time is optimized per band. Using Konika Minolta CS2000 spectroradiometer and a luxmeter, the radiance and luminance of each LED were measured and multiplied by the exposure time, giving the dose of light in $\text{J} \cdot \text{sr}^{-1} \cdot \text{m}^{-2}$ and lux · hr, respectively (see Table 1). By monitoring the light dosage, our current image captures become comparable to future captures, whereby we can assess the fading triggered by the digitization process.

Fig. 4 Our autochrome digitization setup is non-invasive and offers flexibility in adjusting the distance between the photograph and the camera

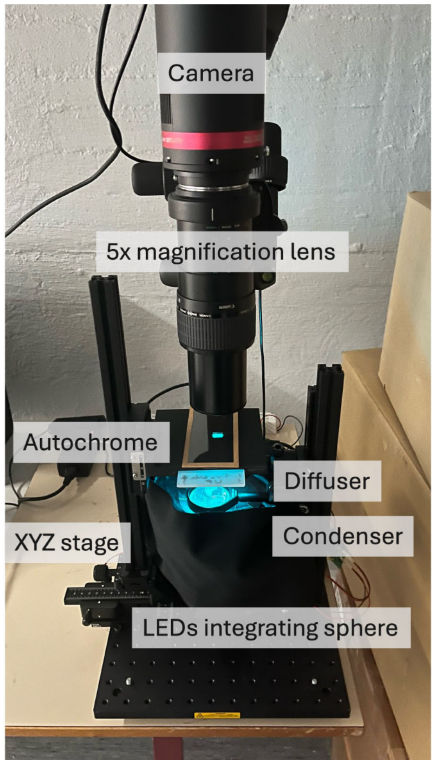

(a) Multispectral Imaging Setup.

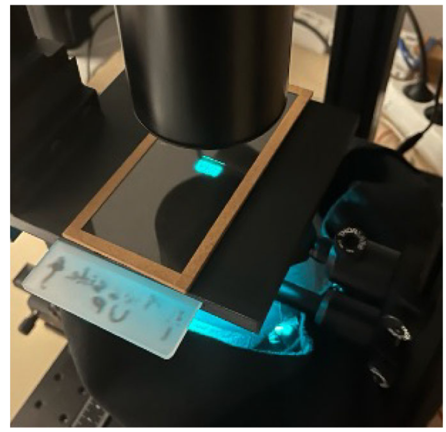

(b) Setup closeup - Autochrome plate on holder, with black cover to minimize stray light and exposure.

Fig. 5 Emission peaks of three of the LEDs, centred at red 446 nm, 520 nm, and 626 nm, coincide with the locations where the absorption cross-talk between the blue, green, and red dyes is minimized

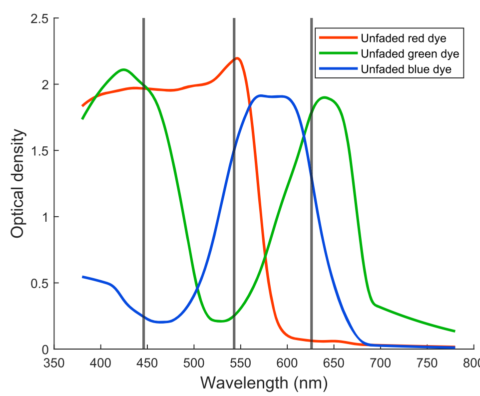

(a) The optical densities of the dyes in an unfaded autochrome, as measured by [9]. The gray vertical lines represent the peak of the LED emission bands in our system, that are used to separate the dyes.

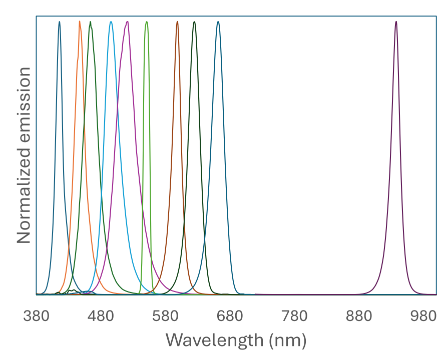

(b) Emission of all the LED lights in our imaging system, which span the visible and near-infrared range.

3.4 Silver/dye decoupling with band subtraction

Our approach leverages both the transparency of the dyes in the infrared spectrum and the precise selection of specific spectral bands in the visible range. Despite scattering effects caused by silver particles in the photographic emulsion, we tested a simplified model that considers only absorption. Thus, we can work in the additive absorption domain, with simple subtractions between the optical densities ($\mathrm{OD} = -\log_{10} T$), with the following equation:

$$\mathrm{OD}_{\mathrm{dye}} = \mathrm{OD}_{\lambda_{\mathrm{visible}}} - \mathrm{OD}_{\lambda_{\mathrm{infrared}}}, \tag{1}$$

where $\mathrm{OD}_{\lambda_{\mathrm{infrared}}}$ corresponds to the optical density of the image captured at $\lambda_{\mathrm{infrared}} = 940\mathrm{nm}$, and $OD_{\lambda_{\mathrm{visible}}}$ to the optical density images captured at $\lambda_{\mathrm{visible}} \in \{626\,nm; 520nm; 446nm\}$ that correspond to the red, green and blue spectral ranges, respectively. We chose these specific spectral bands because they are the ones where the optical density of one dye out of the three types (red-orange

Table 1 Light dosage for the multispectral captures of the autochromes

	415 nm	446 nm	466 nm	492 nm	520 nm	543 nm	599 nm	626 nm	658 nm
Luminance (lux)	68.80	357.67	823.00	787.33	2543.67	102.50	978.00	842.00	1118.67
Radiance ($W \cdot sr^{-1} \cdot m^{-2}$)	6.77	10.70	8.60	1.41	3.57	0.11	2.98	6.81	11.01
Exposure time (s)	1.43	0.73	0.74	1.95	1.48	52.65	4.71	2.91	0.46
Light dose ($lux \cdot hr$)	0.027	0.072	0.169	0.426	1.046	1.499	1.28	0.681	0.143
Radiation dose ($J \cdot sr^{-1} \cdot m^{-2}$)	9.68	7.81	6.36	2.75	5.28	5.79	14.04	19.82	5.06

R, green G and blue-violet B) is minimum, and there is the smallest cross-talk with the optical densities of the other two. Thus, applying Eq. 2 with the three visible bands yields masks that show the spatial distribution of each dye

$$\begin{aligned} \mathrm{OD}_R &= \mathrm{OD}_{626\ \mathrm{nm}} - \mathrm{OD}_{940\ \mathrm{nm}} \\ \mathrm{OD}_G &= \mathrm{OD}_{520\ \mathrm{nm}} - \mathrm{OD}_{940\ \mathrm{nm}} \\ \mathrm{OD}_B &= \mathrm{OD}_{446\ \mathrm{nm}} - \mathrm{OD}_{940\ \mathrm{nm}} \end{aligned} \tag{2}$$

Because the cross-talk between the dyes and the silver emulsion is not the same for the three dyes, the contrast of each mask is adjusted, resulting in a processed mask, noted hereon $\mathrm{Mosaic}_{\mathrm{dye}}$. The units of $\mathrm{Mosaic}_{\mathrm{dye}}$ are correlated to optical density quantities, but are not linearly representing them anymore. This is done by adjusting the histogram of each mask by finding the lower and upper limits, where the percentage of the data below the lower limit is saturated to low intensities and the percentage of the data above the upper limit is saturated to high intensities. These limits are optimized per autochrome and per mask by ensuring there are no overlapping areas between the masks and that the maximum levels are similar. For the autochromes in this paper, the lower limits are between 25% and 35% of the lower pixel values, and the upper limits are between the 99% and 100% highest pixel values. The output low and high intensities are 0 and 0.99, respectively.

In addition, we generate a mask of the carbon element by taking the complement of the dyes mosaic in the transmittance domain, with Eq. 3. This is because our system is not capable of directly resolving the carbon elements filling the spaces between the dyes and so, there is optical mixing between the carbon elements and the dyes. For this reason, the carbon elements are tinted with the colour of the adjacent dye particles. Thus, we compute a carbon map in relation to each dye:

$$\mathrm{Carbon}_{\mathrm{dye}} = 1 - \mathrm{Mosaic}_{\mathrm{dye}}, \tag{3}$$

3.5 Silver/dye decoupling with spectral unmixing

The acquisition of nine spectral bands in the visible spectrum enables a sufficiently good spectral accuracy [17] to facilitate the application of spectral unmixing techniques. The latter are traditionally used to find abundance maps of the endmembers (pure materials) in a scene [18]. For the autochromes, we consider as endmembers the three dyes. At the same time, because the silver and carbon are only modulating the contrast of the image, we assume that they will be embedded either in the abundance maps or in the residual of the unmixing model. Hence, we apply the same rationale, aiming to separate the three dyes in the image from the monochromatic signals given by silver and carbon. More precisely, for each autochrome capture, we build a multispectral cube by considering only the bands in the visible range. Then, for the selection of the endmembers, we select an area in the capture devoid of silver. From this no-silver area, we sample the individual spectrum for each of the red, green and blue dyes, and then finally average to get a characteristic spectral signature for the optical density of each dye. By operating in the additive absorption domain, we assume a linear spectral mixing model. In other words, we consider every pixel ij in the multispectral cube to be a linear combination of the three dyes:

$$\mathrm{OD}_{\mathrm{cube}} = \mathrm{ab}_R^{ij} * \mathrm{OD}_R + \mathrm{ab}_G^{ij} * \mathrm{OD}_G + \mathrm{ab}_B^{ij} * \mathrm{OD}_B + \mathrm{residual}^{ij} \tag{4}$$

with $i = 1..N$ and $j = 1..M$, where N is the number of rows and M is the number of columns in the multispectral image. The aim is to find the abundance ab of each dye in every pixel ij that will finally result in the distribution of each dye over the whole extent of the image, which is called abundance map. The abundance is a quantity proportional to the concentration, without having absolute values or a standard measurement unit. Equation 4 is solved with the least-square minimization method [18], where the objective function is the squared absolute difference between the initial multispectral cube and its estimation given the linear mixing model, $|OD_{cube} - \widehat{OD}_{cube}|^2$, while preserving the abundances as positive numbers.

Afterwards, we can reconstruct the multispectral cube by multiplying the abundance maps with the spectral signatures of the dyes, as follows:

$$\widehat{\mathrm{OD}}_{\mathrm{cube}} = \mathrm{ab}_R^{ij} * \mathrm{OD}_R + \mathrm{ab}_G^{ij} * \mathrm{OD}_G + \mathrm{ab}_B^{ij} * \mathrm{OD}_B, \tag{5}$$

The reconstructed cube is a modelled version of the initial multispectral cube. Thus, the residual error is given by the difference between the initial multispectral cube and the reconstructed cube:

$$\text{residual}^{ij} = \text{OD}_{\text{cube}} - \widehat{\text{OD}}_{\text{cube}} \tag{6}$$

The abundance maps isolate the dye mosaic, while the residual segments the silver emulsion layer.

3.6 Colour restoration

The spectral transmittances of the newly fabricated, unfaded dyes used for colouring the potato starch granules in the autochrome were previously measured by Lavédrine and Gandolfo [8] on a historical autochrome in good condition and they are graphically represented in Fig. 5a.

After obtaining the colour mosaic for each dye with the band subtraction method, as explained in the previous paragraph, we assign to each of the three dye maps the original colours as rendered by integrating the spectral transmittances provided by [8]. This way, we obtain a restored or unfaded colour mosaic. At this point, to achieve the restoration of the entire plate, we recombine the new colour mosaic with the current silver layer (assuming that the silver layer is stable and has not changed nor degraded) and the carbon map.

Similarly, by following the spectral unmixing approach, we obtained abundance maps by decomposing the multispectral cube of each autochrome into its pure dyes following Eq. 4. The optical densities of dyes in a faded autochrome would typically be lower and flatter than those in an unfaded autochrome, as shown in Fig. 9c. Consequently, we create another cube by multiplying the abundance maps with the optical densities of the reference, unfaded dyes. This results in the restored colour mosaic. Then, to add spatial details, we sum the restored colour mosaic with the residual given by Eq. 6 that encapsulates the silver and carbon:

$$\text{OD}_{\text{restored cube}} = \text{ab}_R^{ij} * \text{OD}_{\text{Ref }R} + \text{ab}_G^{ij} * \text{OD}_{\text{Ref }G} + \text{ab}_B^{ij} * \text{OD}_{\text{Ref }B} + \text{residual}^{ij} \tag{7}$$

After obtaining the restored multispectral cube, we render the colours for the CIE 1931 2° standard observer and the D50 standard illuminant. Finally, we apply the Rec. 2020 colour profile, which is an image viewing encoding that follows the recommendations of the normative reference ITU-R BT.1886 [19]. Rec. 2020 implies a gamma encoding with $\gamma = 1/2.4$.

4 Results and discussion

4.1 Spectrophotometric characterization of the selected autochromes

We collected point measurements with the high-magnification spectrophotometric system presented in Sect. 3.2. For each autochrome, we randomly sampled approximately seven granules belonging to each of the three dye groups and gathered their spectral transmittance. Afterwards, we averaged the individual measurements to obtain representative spectral signatures for the primary dyes in the test autochromes, as displayed in Fig. 6. The colour of the plotted line is the true colour of the dyes, rendered for CIE 1931 2° standard observer and D50 standard illuminant. To view the variations of all the dyes, we plotted all the individual point measurements in a CIE u′v′ chromaticity diagram shown in Fig. 7. The measured granules span a wide range of chromaticities, which might be due to different manufacturing and/or different ageing states of the autochromes. The colours of the blue dyes are less saturated compared to the reference blue dye of [8]. This was somewhat expected considering that the blue dye is the most fugitive. On the other hand, for the red and green dyes, some of our measurements very closely approach the saturation levels of the corresponding reference dyes.

4.2 Multispectral imaging of the selected autochromes

The test autochromes were imaged using the setup presented in Sect. 3.3. Figure 8 shows an area of each autochrome where the silver emulsion is assumed to be transparent, at 100% magnification. The resolution of the imaging system is sufficient to resolve the individual dyes, revealing their current state of conservation. We see that each of the autochromes presents different levels of fading, and the colours of their primary dyes slightly vary from one plate to another. The first autochrome, “Couple by the lake”, is the least faded autochrome. It is known that the blue-violet dye is the least stable one; however, we see that in this case, the blue-violet dyes are quite dark. The opposite is true in the case of the “Poppy field” and “Harrogate shop window” autochromes, which show lighter coloured blue-violet dyes. Moreover, the green dyes of the “Harrogate shop window” are also quite light in comparison with the other autochromes. In the case of the “Gruyere” autochrome, the blue-violet dyes are duller than those in the other autochromes.

The optical densities of the dyes of each test autochrome were computed as an average of the area in Fig. 8. This is presented in Fig. 9. It is important to mention that there is a difference, especially in magnitude, if we compare these optical densities with the ones obtained from the spectrophotometric measurements displayed in Fig. 6. There are several reasons for this. First, in the spectrophotometric experiment, we randomly chose the granules to be measured, without aiming exclusively for areas not covered by silver, as is the case with the granules chosen for endmembers in Fig. 9 extracted from the multispectral imaging. Then, in the

Fig. 6 Spectral signatures of the dyes for each autochrome, as measured with the point measurement setup. Around seven granules corresponding to every dye group were randomly chosen, measured, and then averaged. Curves are rendered in the true colour of the dyes. The noise present in the short-wavelengths is due to the low emission signal of the tungsten-halogen light source before 450 nm

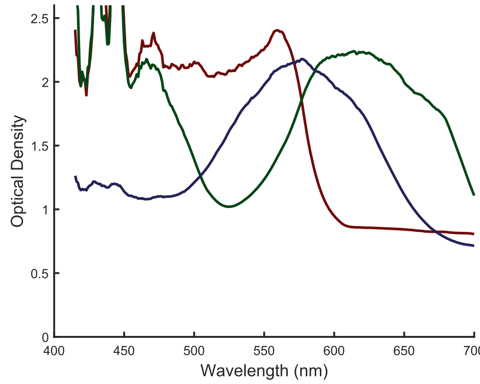

(a) Spectrophotometric characterization of the dyes in the "Couple by the lake" autochrome

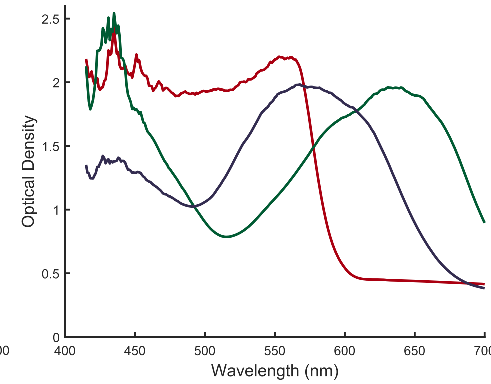

(b) Spectrophotometric characterization of the dyes in the "Gruyere" autochrome

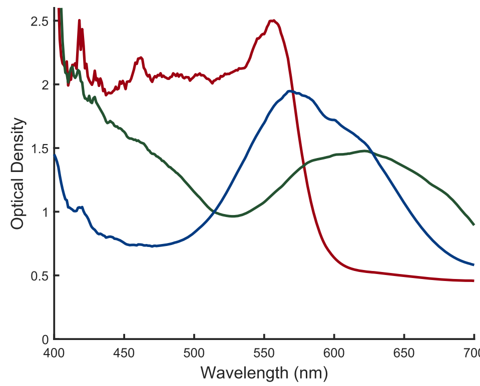

(c) Spectrophotometric characterization of the dyes "Harrogate shop window" autochrome

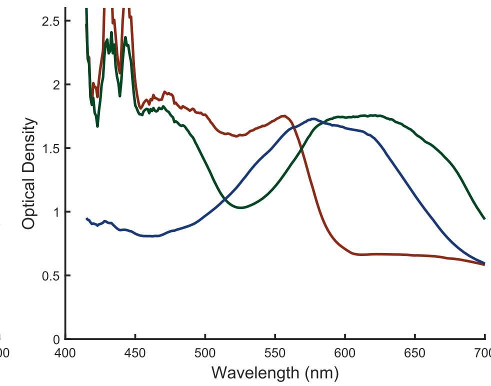

(d) Spectrophotometric characterization of the dyes "Poppy field" autochrome

Fig. 7 CIE u′v′ chromaticity plot of the dyes in our test autochromes, as individually measured with the point spectrophotometric measurements, and the dyes in the reference autochrome. Each marker shape corresponds to a specific autochrome

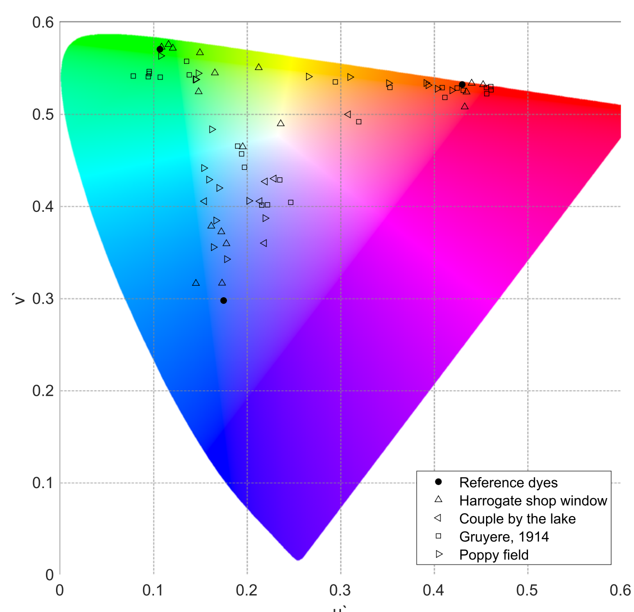

multispectral image, thanks to the spatial resolution, we have a bigger pool of individual granules to average from than that of the spectrophotometric measurements (approximately 7 measurements/dye group).

The least faded autochrome seems to be "Couple by the lake", while the most faded seems to be "Gruyere" and the "Harrogate shop window", judging by the drop in magnitude and the flattening of the spectral shape of the dyes. Compared to the reference optical densities in Fig. 5a, the maximum optical density of the dyes is lower, meaning that they absorb less light, but also the

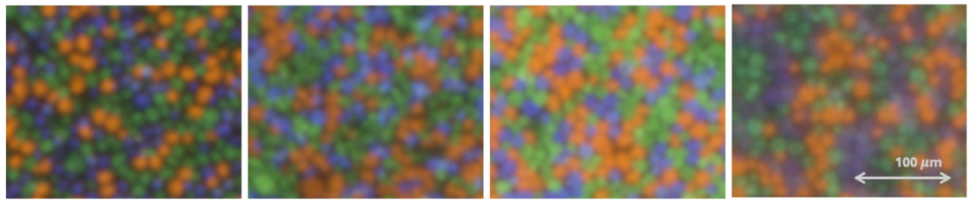

Fig. 8 Dyes uncovered by the silver emulsion, cropped from the colour images of the four autochromes: Couple by the lake, Poppy field, Harrogate shop window, Gruyere

Fig. 9 Spectral signatures of the pure dyes for each autochrome. Curves are rendered in the true colour of the dyes

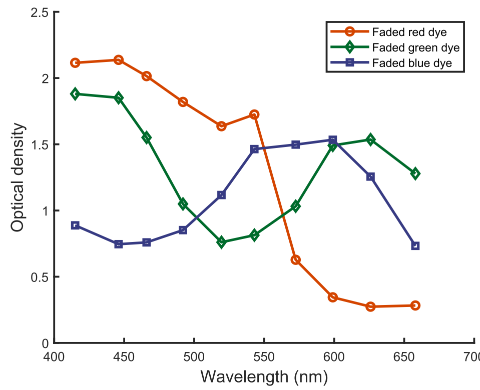

(a) Spectral signatures of the pure dyes in the "Couple by the lake" autochrome

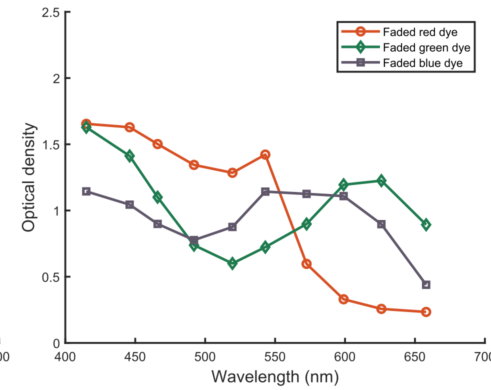

(b) Spectral signatures of the pure dyes in the "Gruyere" autochrome

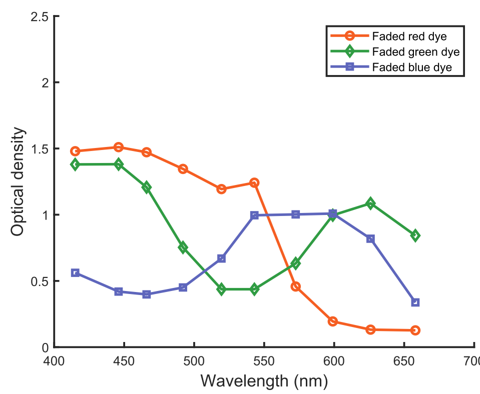

(c) Spectral signatures of the pure dyes in the "Harrogate shop window" autochrome

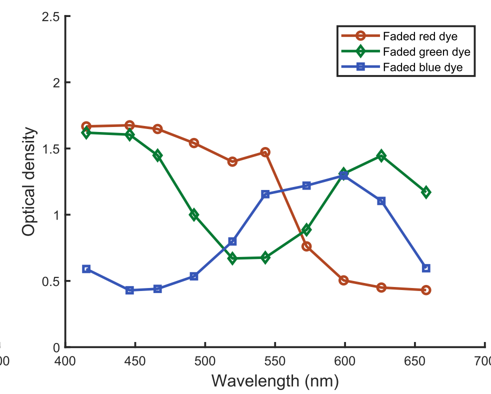

(d) Spectral signatures of the pure dyes in the "Poppy field" autochrome

minimum optical density is higher, meaning that they transmit less light as well. The overall effect this has on the autochrome is a loss of contrast and desaturated colours.

Figure 10 shows the CIE u′v′ chromaticity diagram of the dyes of our autochromes, as well as the reference, unfaded autochrome. Each autochrome is represented by a different marker, and the marker colour represents the dye, either orange-red, green or violet-blue. The reference dyes cover a large space of the chromaticity diagram. As expected, each dye shows different degree of fading. Violet-blue is the most light-sensitive dye and as such has the most significant change. Each autochrome has a different degree of fading, "Gruyere, 1914" being the most faded, followed by "Harrogate shop window", "Couple by the lake", and finally "Poppy field". In the case of the orange-red and green dyes, the fading is much smaller and there are no very large differences between the four test autochromes. Here, it must be noted that the reference spectra come from an autochrome in *good condition*, which is a subjective statement. It is known that each batch of autochromes had a different colour rendering, and even a single plate could have mixed dyed starches, with different levels of saturation and hue. Thus, we are only using this as a candidate for a possible colour restoration.

4.3 Colour restoration based on band subtraction

Following the method explained above, the band subtraction method takes advantage of the infrared image, which we assume to only capture the silver emulsion. This image is subtracted from the three bands identified for each dye (Fig. 11a–c). The resulting image is the mosaic or mask of dyes (Fig. 11d–f). As observed, subtracting the silver emulsion image significantly removes spatial information from the band images. However, minor imperfections remain, such as a faint ghost-like artefact of the woman's silhouette

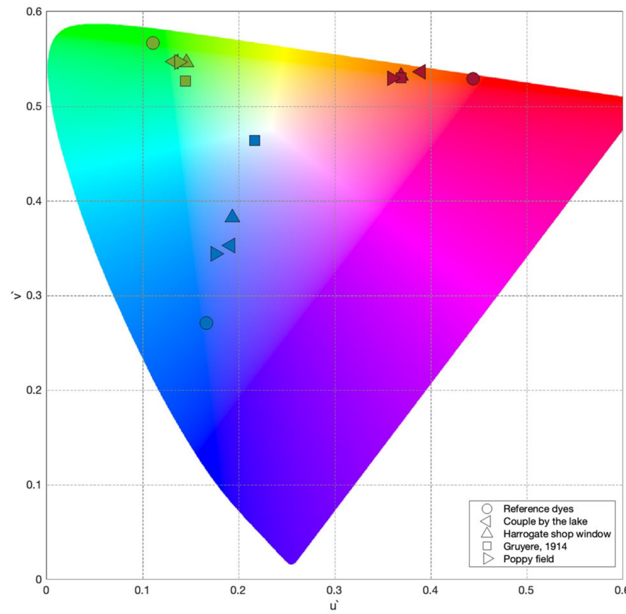

Fig. 10 CIEu′v′ chromaticity plot of the dyes measured from our autochromes, and of the reference autochrome. The different marker shapes represent each autochrome, and the colour of the marker indicates to which dye it belongs

Fig. 11 Process to decouple the dye mosaic from the silver image by band subtraction. The first row shows the image at the selected band for each dye. The second row shows the result of the separation by subtracting the silver image (infrared). The third row shows the final dye mosaic, after contrast enhancement

(a) Image corresponding to orange-red band at 626 nm.

(b) Image corresponding to green band at 520 nm.

(c) Image corresponding to violet-blue band at 446 nm.

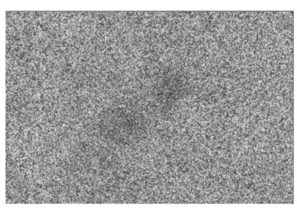

(d) Orange-red mosaic.

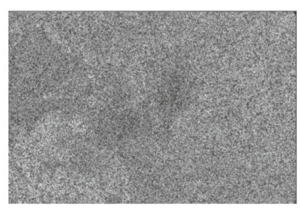

(e) Green mosaic.

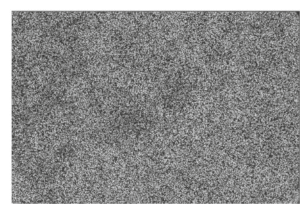

(f) Violet-blue mosaic.

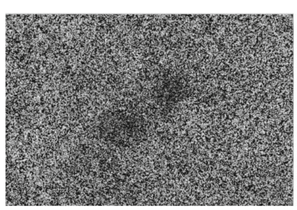

(g) Orange-red mosaic after contrast enhancement.

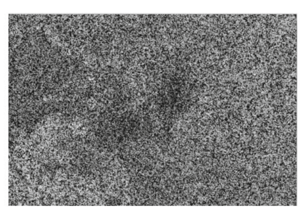

(h) Green mosaic after contrast enhancement.

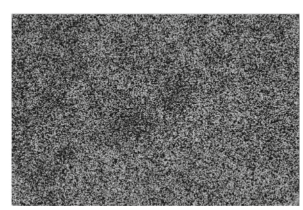

(i) Violet-blue mosaic after contrast enhancement.

in the mosaic images (especially the green one), likely due to scattering effects not accounted for in our model. Additionally, the lens is not well-suited for infrared radiation, resulting in stray light that introduces an artefact in the centre of the images. To minimize cross-talk between dyes, the contrast of the masks is enhanced, ensuring that each mask accurately represents only the dyes of interest (Fig. 11g–i).

The virtual separation and restoration of the autochrome is shown in Fig. 12. The multispectral image, containing the transmittance of the autochrome, is rendered to true colour for the CIE 1931 2° standard observer and the D50 standard illuminant. Finally, we apply the Rec. 2020 colour profile, which gives the original colour image in Fig. 12a. The separation of the dye layer from the silver emulsion is done following the steps above. The silver emulsion is presented in Fig. 12e. Figure 12b shows the true colour rendering of the faded dye mosaic after the separation from the silver emulsion. As seen in the image, the colour mosaic is very dark and has a

Fig. 12 Restoration based on band subtraction. For visualization purposes the levels of the colour images have been adjusted to a maximum value of 140, to enhance their contrast and visibility

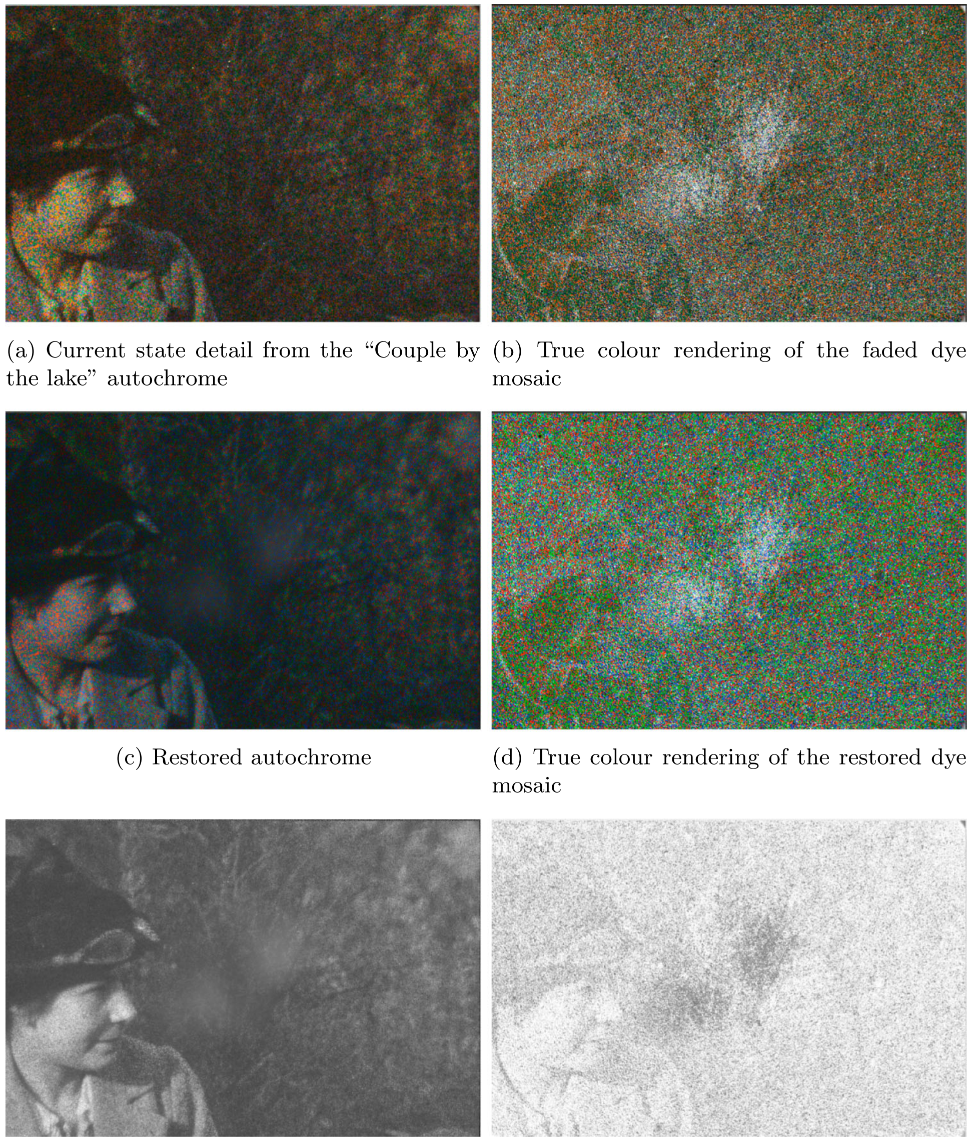

(a) Current state detail from the "Couple by the lake" autochrome
(b) True colour rendering of the faded dye mosaic
(c) Restored autochrome
(d) True colour rendering of the restored dye mosaic
(e) Silver layer
(f) Carbon layer

sepia tint, because, as mentioned before, the orange-red dye is the least fugitive dye, and thus, the most present colour. This is also evident in the colour image of the autochrome.

For the virtual restoration, the optical densities of the reference dyes are assigned to their corresponding mask, creating a restored dye mosaic. This is shown in Fig. 12d. As we can see, the result is much brighter, and the distribution of orange-red, green, and violet-blue dyes is more uniform, there is no longer an orange-red dominance.

Finally, to reconstruct the entire autochrome, the carbon image is created by finding the complement of the colour mosaic, shown in Fig. 12f. Then, the three images (restored dyed mosaic, silver layer and carbon layer) are added in the absorbance domain, converted back to transmittances, and calculated into colour coordinates following the same steps as for the original image.

4.4 Colour restoration based on spectral unmixing

For each multispectral image of the autochromes in our study, we select an area where silver is not present (Fig. 8), and hence is the basis to extract the average signatures of the red, green, and blue dyes in the visible spectral range (Fig. 9). These signatures are the endmembers and become input to the spectral unmixing method. As a result, we obtain the spatial distribution of the dyes in the whole image, in the form of abundance maps, as shown in Fig. 13 for the woman detail in the "Couple by the lake" autochrome whose dyes are plotted in Fig. 9a. Furthermore, we decompose the dyes from the silver and carbon signals (see Fig. 14). Because carbon is optically mixed with the colour of the adjacent dyes, it is embedded in the abundance maps of the dyes. In addition, the residual between the original multispectral image and the image estimated with the unmixing model yields the silver layer.

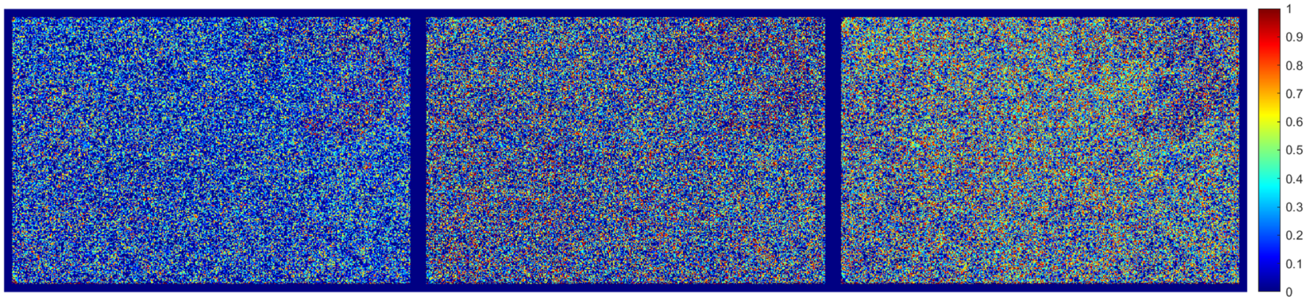

Fig. 13 Abundance maps for the red, green, and blue dyes, obtained by spectrally unmixing the woman detail in the "Couple by the lake" autochrome, with endmember dyes plotted in Fig. 9a

This is obvious by comparing the residual image in Fig. 14e with the infrared image in Fig. 14f. Because under infrared light the colour dyes are transparent, the respective image captures the silver emulsion layer. However, due to the lens of our system, which is not optimized for infrared emission, the infrared pictures are contaminated by an optical halo-shaped artefact that appears at the centre of the image. The residual image has the same outline as the infrared image, but has the advantage of not having the optical artefacts present in the latter. This makes the residual image a denoised and sharper representation of the silver layer than the straightforward infrared capture. Nevertheless, in the future, the latter can be improved by furnishing our imaging system with a more costly infrared-extended, apochromatic lens, provided that financial resources are available.

Then, by multiplying the abundance maps with the endmember signal, we recreate the original cube, by only taking the dyes and carbon elements into account. In Fig. 14b, we can see the colour rendering of the recreated cube, which shows the faded dye mosaic. Similar to the mosaic yielded by the band subtraction method, a less obvious ghost-like artefact of the woman's silhouette appears in this method's dye mosaic. Most probably, the reason for this artefact lies in the scattering effects that we do not account for in our models. To compose the restored dye mosaic, we mix the abundance maps with the spectra of the unfaded dyes (displayed in Fig. 5a). Finally, by adding the silver layer as represented in the residual image (Fig. 14e), to the restored dye mosaic in Fig. 14d, we can visualize a restored version of the autochrome in Fig. 14c. For the sake of brevity, we show examples of the intermediate results (abundance maps, faded and unfaded dye mosaics, residual) for only one autochrome.

4.5 Discussion

In Fig. 15, we gathered the digital restorations for selected details in the four autochromes, derived from both our methods: band subtraction and spectral unmixing. The various details were chosen based on their chromatic content, as we want to show that we are able to rejuvenate a wide range of colour combinations, at different stages of fading, and contextualized in different semantic compositions. Nevertheless, in Fig. 16, we go beyond the detail-level taken from a single image capture, and we assemble eight image captures that cover a larger portion from an autochrome. This montage was created by performing image stitching, where SIFT features are extracted in order to automatically find the connection points between two adjacent images.

The first visual effect we notice when looking at the restorations of all four autochromes in Fig. 15 is a more balanced distribution of colours with respect to the current state. For instance the woman detail in "Couple by the lake" (Fig. 16a) and the window in "Gruyere" (Fig. 15k) have a strong orange cast in the current state that is removed in the restoration. This is intuitive considering that the blue dye is the one most fugitive, while the red-orange is the most lightfast. The restorations balance out the orange domination, by injecting blue back in the pictures. Other striking chromatic effect can be observed in the "Harrogate shop window" where the hat of the doll recovers its green hue almost unperceivable in the current state (Fig. 15e), and where the blue flower regains not only its saturation, but also its veins and folds that are now more visible thanks to the increased colour contrast. Similarly, in the "Poppy field", we can now see redder poppies (especially in Fig. 15i) and significantly bluer flowers.

Another expected effect of the restorations is to grasp an overall darker appearance, because the original dyes have higher optical densities than the faded ones. Indeed, the restorations are darker than the current state. However, to achieve visibility, it was necessary in some cases to increase the brightness of the images by applying histogram stretching. We noticed that the spectral unmixing restorations are slightly brighter than the band subtraction ones, while still remaining darker than the current state. A possible reason for this discrepancy could be the fact that the abundance maps in the spectral unmixing approach, manage to better encode the relative contrasts between the dyes in a given scene and thus output a more locally adjusted brightness. Then, the spectral unmixing restorations are sharper than the band subtraction ones, and this is mainly due to the optical artefact present in the infrared image which is used in the band subtraction.

To add a quantitative comparison of our two restoration methods, we report the colourfulness metric proposed by Hasler and Suesstrunk [20] for the current state images of the autochrome details and their associated two restorations. The colourfulness metric indicates the perceptual visual quality of an image. Mathematically, it is a linear combination of the standard deviation and mean of the opponent blue-yellow and red-green colour space. According to the numerical values of the colourfulness metric, a qualitative

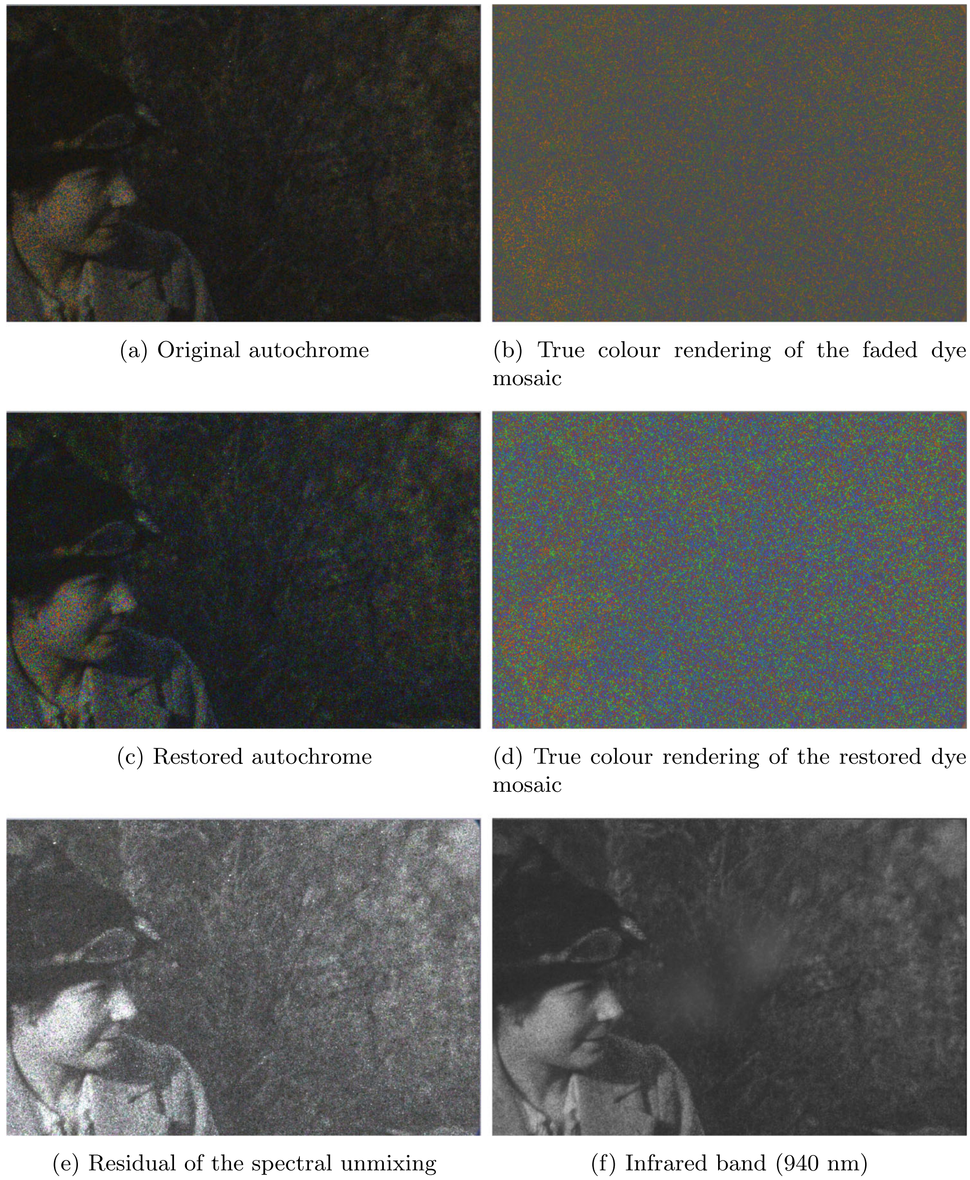

Fig. 14 Restoration with the spectral unmixing method (c) pulls up the faded blue colours in the original image, obvious especially in the coat area, and increases the overall contrast. Moreover, the dyes are well decoupled from the silver layer. The restoration is sharper, as the spectral unmixing denoises the image through dimensionality reduction. This is particularly obvious if we compare the silver layer (f) as given by the infrared image (that has several artefacts and is affected by blurriness) with the residual of the spectral unmixing (e)

colourfulness attribute can be assigned. Thus, values that exceed 109 suggest an *extremely colourful* image; values between 82–109 correspond to *highly colourful* images; values between 59 and 82 show a *quite colourful* image; values in the range of 45 and 59 are *averagely colourful*; values in the range of 33 and 45 are *moderately colourful*; values between 15 and 33 are *slightly colourfu*l and values below 15 indicate *not colourful* images. The colourfulness values for the images in Fig. 15 are reported in Table 2. Generally, we can see that the spectral unmixing method leverages the colourfulness of the current-state images, and climbs up to one level in the qualitative attribute scale (with the exception of the detail in the "Couple by the lake" autochrome). Conversely, the band subtraction method does not change the qualitative colourfulness scale. Even more, it decreases the attribute of the "Poppy field" autochrome from *quite colourful* to *moderately colourful*. When restoring the colour of cultural heritage objects, we deal with the lack of an absolute ground-truth, and so one of the pitfalls is to "over-restore" or not knowing where to stop the restoration process. In this sense, the colourfulness metric is a way to verify that the results do not "over-restore" the current-state autochromes and may hence be considered a way to cope with the lack of ground-truth. The reported metrics for our selected autochromes indicate that, indeed, the change is going up at most one additional level in the hierarchy of colourfulness, which proves that our proposed solutions do not "over-restore".

4.5.1 Limitations

There are a few limitations to our proposed approaches. Firstly, the acquisitions are done at a very high magnification. This is required since we need to resolve individual dye granules to separate them from the silver emulsion. As a result, only a very small

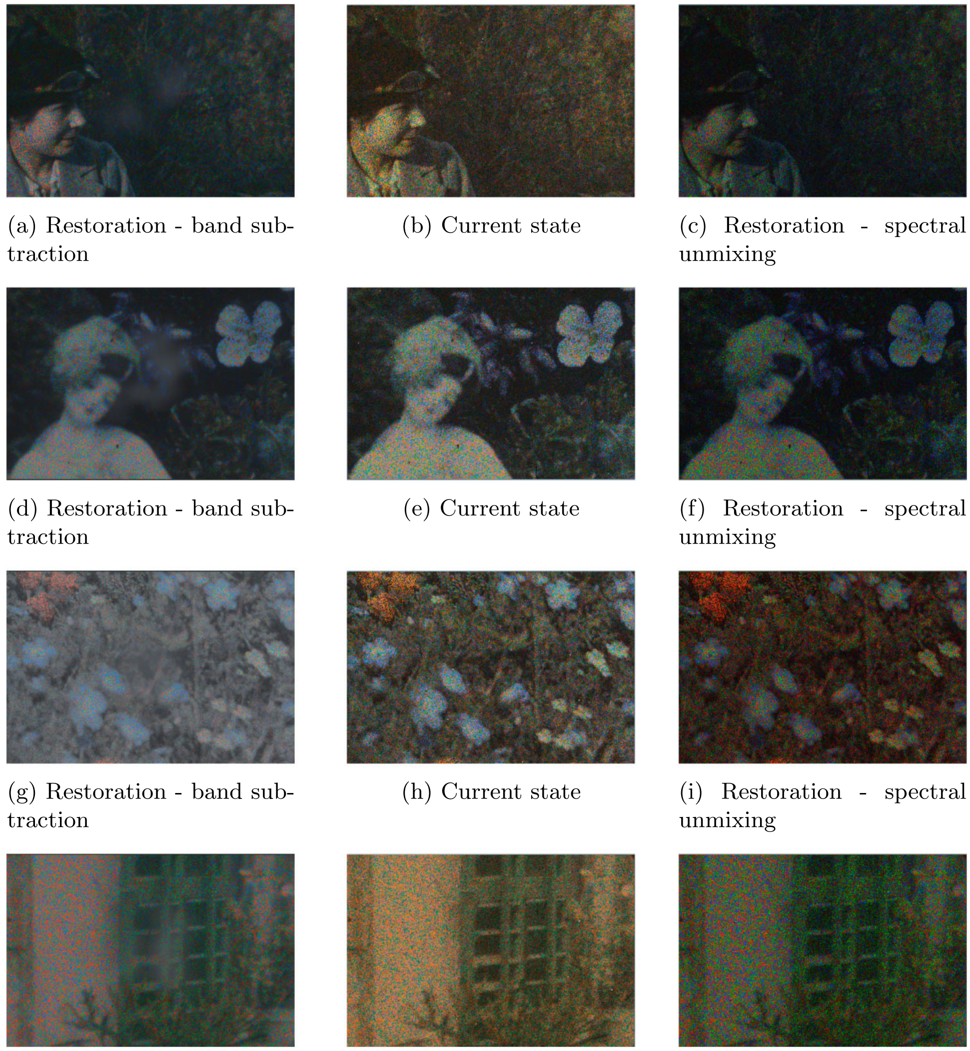

(a) Restoration - band subtraction (b) Current state (c) Restoration - spectral unmixing

(d) Restoration - band subtraction (e) Current state (f) Restoration - spectral unmixing

(g) Restoration - band subtraction (h) Current state (i) Restoration - spectral unmixing

(j) Restoration - band subtraction (k) Current state (l) Restoration - spectral unmixing

Fig. 15 Colour restoration of the test autochromes presented side by side to the current state of the photographs. The images corresponding to the current state and the band subtraction restoration were manipulated here for visualization purposes. Thus, brightness was increased by stretching the histogram

Table 2 Colourfulness metric computed for the images shown in Fig. 15 that represent the autochrome details in their current state, and their restored states

	Autochrome			
Colourfulness metric	**Couple**	**Poppy field**	**Harrogate**	**Gruyere**
current state	71.07	76.29	71.43	85.76
restoration Band Subtraction	66.26	43.33	60.64	88.74
Δ wrt current state	-4.80	-32.96	-10.79	2.98
restoration Spectral Unmixing	61.70	89.90	85.89	112.68
Δ wrt current state	-9.37	13.61	14.46	26.92

Overall, the spectral unmixing method increase to a higher extent the colourfulness of the current state images, than the band subtraction method. The cells in darker shade of green correspond to an *extremely colourful* image, those in medium green shade correspond to a *highly colourful* image, and those in light green to *quite colourful* images

section of the autochrome is virtually restored. The granularity of the autochrome at this magnification is much more visible than when looking at the autochrome in normal conditions, even with a magnifying glass. This has an impact on the optical mixing effect that happens normally when viewing the autochromes, and influences the accurate interpretation of the restored colours.

Another limitation related to the high magnification of these images is the amount of data produced, and that would be required to restore a whole autochrome plate. As shown in Fig. 16, it is possible to acquire tiles of the autochrome and stitch them together. However, this process would generate an extremely large amount of computation and data.

It is important to mention that due to the manufacturing process characteristic to autochromes, which is of a rather crafting nature, no two batches of autochromes are fully alike. Therefore, converging autochromes of different production to the same set

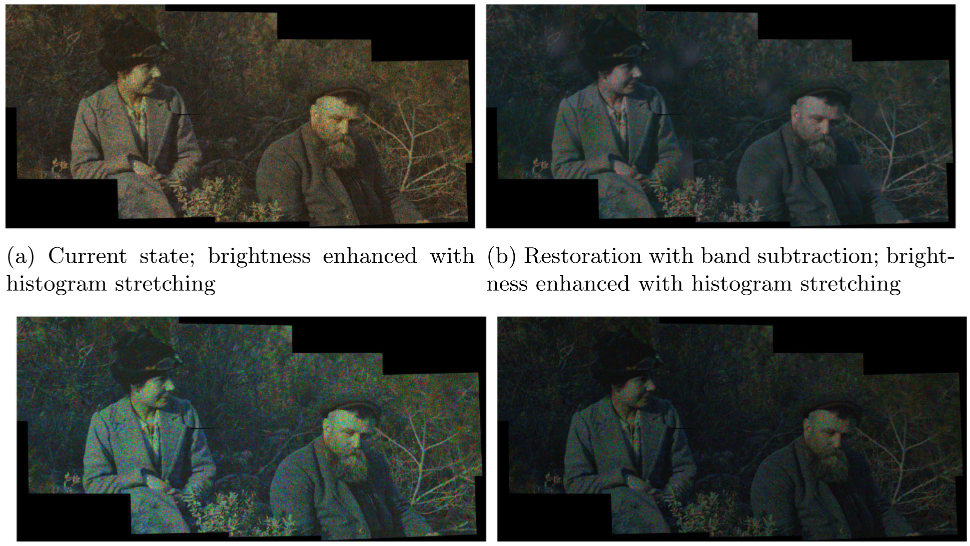

(a) Current state; brightness enhanced with histogram stretching
(b) Restoration with band subtraction; brightness enhanced with histogram stretching
(c) Restoration with spectral unmixing; brightness enhanced with histogram stretching
(d) Restoration with spectral unmixing; no brightness enhancement

Fig. 16 Presentation of results for a larger scene in the "Couple by the lake" autochrome, created by stitching eight individual image captures. The purpose of this integrated result is to mitigate the graininess effect in single captures due to the high-magnification, and to prove that our methods are functional for the entire autochrome, not just a detail

of reference dyes might not be entirely correct. In addition, autochrome chemists and engineers have been experimenting a lot with the recipes and formula of the dyes in order to get more vivid colours, which becomes yet another cause of inaccuracy of using a single set of reference dyes. In the future, we plan to account for this by trying to uncover the reference dyes for each autochrome in particular, by measuring the dyes covered by the black frame typically protecting most of the autochromes (see Fig. 2). Naturally, in this case, we would assume that by not being exposed to light, the dyes under the black frame are as much as possible the original ones. However, removing the frame is an invasive procedure that might incur damage to the autochrome.

Moreover, our reference dyes come from a historical plate in good condition. Another idea for improvement would be to recreate the formula of the integrated dyes starting from measurements of the various constituent colourants in each dye. Casella et al. [7] recreated the solutions for each colourant in the autochrome dyes, and spectrally measured their reflectance. In a second iteration of our paper, we plan to create renderings by using the measurements of Casella et al. [7] in addition to the ones of Lavédrine and Gandolfo [8] considered in the current study.

4.5.2 Contribution to the autochrome demonstrator

While our work primarily falls within the realm of scientific research, the proposed methods also have immediate artistic application. In fact, our silver/mosaic decoupling methods were used to create the "Autochrome Demonstrator" (Fig. 17) [21], an interactive and educational tool designed for museum displays. The Demonstrator highlights the multilayered structure of autochromes through a series of prints, which separately depict the silver emulsion layer and the colour screen. These prints are arranged in an optical system that allows viewers to visually blend the layers, reconstructing a complete autochrome image. Additionally, the impact of colour restoration is demonstrated using two interchangeable colour screens: one representing the faded state of historical autochromes and the other showcasing the restored version. The Demonstrator has been exhibited and evaluated at several events, including the InArt2024 conference [22] and the SITEM 29 salon [23], where it was presented to experts in the cultural sector.

5 Conclusions and future work

In this article, we proposed a twofolded method for the colour restoration of autochromes. Our solution is versatile and it can be tailored to different types of input data depending on the preferred imaging system that a cultural institution has at hand. More specifically, if only a colour camera setup with limited multispectral capabilities is available, then we propose a variant that only requires one additional image in the near-infrared. This is easily achievable in a commercial colour camera by removing the infrared cut-off filter. Instead, if multispectral imaging is possible, with at least nine spectral bands that sample the visible range of the electromagnetic spectrum, then spectral unmixing can be conveniently employed for the colour enhancement of autochromes, without the need of a specific acquisition in the infrared.

We are aware that the majority of existing digital pictures of autochrome collections come in a plain colour format, without any infrared image, and without the possibility of a re-digitization. For this reason, in the future, we plan to design a style transfer

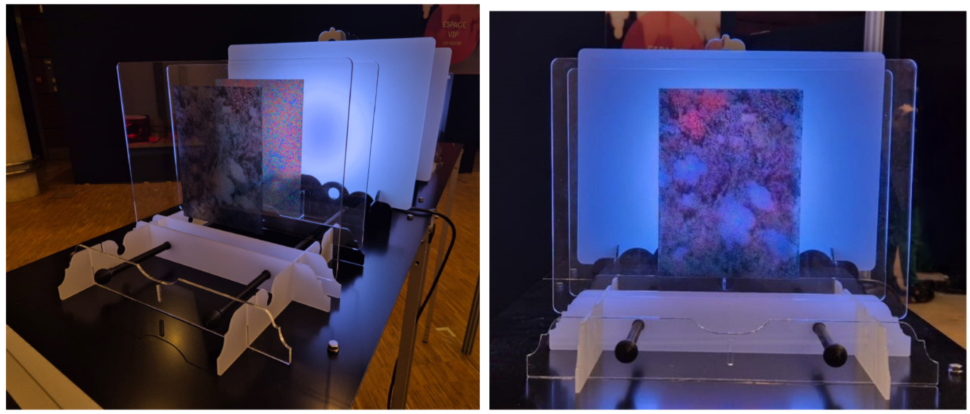

Fig. 17 The Autochrome Demonstrator [21], designed and created by Arthur Clay (HSLU), is an optical system that allows viewers to explore the individual layers of an autochrome (left). By visually aligning and recombining these layers, the viewer reconstructs the full-colour image (right). The printed layers are derived from our processing of the "Poppy field" autochrome

method to associate faded colours with restored colours, by learning many such combinations from our test cases and ultimately generalizing to all autochromes available in museum digital galleries.

Acknowledgements This work was partially funded by the Horizon EU PERCEIVE project (2023–2026), under Grant Agreement Nr. 101061157. We acknowledge Prof. Arthur Clay from HSLU for providing us the first test autochrome, "Couple by the lake" and for designing and manufacturing the Autochrome Demonstrator. In addition, we thank Bertrand Lavédrine and Jan Hubicka for the exchange of knowledge and for their seminal work on early historic photography, which paved the way for ours. The microscopic spectrophotometric measurements became possible with the help of the Health Department in NTNU Gjøvik who lent us the 40× microscope lens and that of John K. Delaney who contributed to a previous version of the system's design.

Funding Open access funding provided by NTNU Norwegian University of Science and Technology (incl St. Olavs Hospital - Trondheim University Hospital).

Data Availability Statement Data sets generated during the current study are available from the corresponding author on reasonable request. The manuscript has associated data in a data repository.

Open Access This article is licensed under a Creative Commons Attribution 4.0 International License, which permits use, sharing, adaptation, distribution and reproduction in any medium or format, as long as you give appropriate credit to the original author(s) and the source, provide a link to the Creative Commons licence, and indicate if changes were made. The images or other third party material in this article are included in the article's Creative Commons licence, unless indicated otherwise in a credit line to the material. If material is not included in the article's Creative Commons licence and your intended use is not permitted by statutory regulation or exceeds the permitted use, you will need to obtain permission directly from the copyright holder. To view a copy of this licence, visit http://creativecommons.org/licenses/by/4.0/.

References

1. L. Casella, K. Sanderson, Display of Alfred Stieglitz and Edward Steichen autochrome plates: anoxic sealed package and lighting conditions. Topics Photogr. Preserv. **14**, 162–167 (2011)
2. C. Hofmann, U. Schoegl, Heinrich Kuehn and photography with autochromes. Topics Photogr. Preserv. **9**, 73–84 (2001)
3. C. Langford, L'apanage de tout photographe. Photographica **88**, 20–35 (2024). https://doi.org/10.4000/11pb3
4. H. Hannouch, Editorial of PhotoResearcher 37: Three-colour photography around 1900: technologies, expeditions, empires. *PhotoResearcher* (2022)
5. S. Wagner, C. McCabe, B. Lemmen, Guidelines for exhibition light levels for photographs. Top. photogr. Preserv. **9**, 127–128 (2010)
6. C.C. Von Waldthausen, Exhibition of photographic materials in library and archive collections, in *ICAICPTE International Symposium, Ljubljana, Slovenia* (2003). http://resources.culturalheritage.org/pmgtopics/2003-volume-ten/10_18_Waldthausen.pdf
7. L. Casella, M. Tsukada, Effects of low-oxygen environments in the light fading of six dyes present in the autochrome color screen. J. Am. Inst. Conserv. **51**(2), 159–174 (2012)
8. B. Lavédrine, J.-P. Gandolfo, *The Lumière Autochrome: History, Technology, and Preservation* (Getty Publications, Los Angeles, CA, 2013)
9. B. Lavédrine, *The study of Autochrome Plate* (Analysis of the dyes. Proceedings of the Imperfect Image; Photographs their past, Present and Future, 1992)
10. H. Arai, M. Tanaka, S. Kubo, A consideration on the color fading of autochrome plate. J. Photogr. Soc. Jpn. **60**(4), 241–247 (1997)
11. A. Günzl, Rekonstruktion von Autochrome-Aufnahmen mit Methoden der Digitalen Bilderarbeitung. PhD thesis, Fachhochschule Köln, Köln (1994)
12. B. Lavédrine, Les autochromes: approche historique et technologique du procédé: étude des problèmes liés à sa conservation. PhD thesis, Paris 1 (1993). https://theses.fr/1993PA010547
13. D. Pfluger, L. Garmsen, G. Trumpy, Modern methods for the visualization of lenticular film colors. Cultura e Scienza del Colore Color Culture and Science **14**(01), 64–72 (2022)
14. G. Barker, J. Hubička, M. Jacobs, L. Kimrová, K. Meyer, D. Peterson, Finlay, Thames, Dufay, and Paget color screen process collections: using digital registration of viewing screens to reveal original color, 2nd edn. Colour Photography and Film: sharing knowledge of analysis, preservation, conservation, migration of analogue and digital materials 2022, vol. 008. Research Culture And Science Books series, Milano (2023). https://doi.org/10.23738/RCASB.008
15. J. Hubička, L. Kimrová, K. Klaeser, S. Manco, D. Peterson, Digital analysis of early color photographs taken using regular color screen processes, in *Color and Colorimetry. Multidisciplinary Contributions, Lecco* (2023), p. 241–248. https://doi.org/10.23738/RCASB.009 . arXiv:2309.09631 [cs]

16. G. Trumpy, J.Y. Hardeberg, S. George, B. Flueckiger, A multispectral design for a new generation of film scanners, in *Optics for Arts, Architecture, and Archaeology VIII*, vol. 11784 (SPIE, Munich, Germany 2021), p. 138–146. https://doi.org/10.1117/12.2592655. https://www.spiedigitallibrary.org/conference-proceedings-of-spie/11784/117840Z/A-multispectral-design-for-a-new-generation-of-film-scanners/10.1117/12.2592655.full
17. R. Shrestha, J.Y. Hardeberg, C. Boust, LED based multispectral film scanner for accurate color imaging, in *2012 Eighth International Conference on Signal Image Technology and Internet Based Systems*, (IEEE, Naples, 2012), p. 811–817. https://doi.org/10.1109/SITIS.2012.122 . http://ieeexplore.ieee.org/document/6395174/
18. N. Keshava, J.F. Mustard, Spectral unmixing. IEEE Signal Process. Mag. **19**(1), 44–57 (2002). https://doi.org/10.1109/79.974727
19. B.T. Series, Parameter values for ultra-high definition television systems for production and international programme exchange. In: Proceedings of ITU-T, Bt. 2020, pp. 1–7 (2012). https://glenwing.github.io/docs/ITU-R-BT.2020-1.pdf
20. D. Hasler, S.E. Suesstrunk, Measuring colorfulness in natural images, in *Human Vision and Electronic Imaging VIII*, (SPIE, San Diego, CA, 2003), vol. 5007, pp. 87–95. https://www.spiedigitallibrary.org/conference-proceedings-of-spie/5007/1/Measuring-colorfulness-in-natural-images/10.1117/12.477378.short
21. https://openspacemuseum.blogspot.com/p/autochrome-demonstrator.html
22. https://www.khm.uio.no/english/research/inart2024/index.html
23. https://www.sitem.fr/